Synergistic effects of *Ret* coding and enhancer loss-of-function alleles cause progressive loss of inhibitory motor neurons in the enteric nervous system

Lauren E Fries,[1] Gabriel Grullon,[1] Lauren Wilkes,[1] Hanna E Berk-Rauch,[1] Aravinda Chakravarti,[1,2,#] and Sumantra Chatterjee[1,2,#]

[1] Center for Human Genetics & Genomics, [2] Department of Neuroscience and Physiology, New York University Grossman School of Medicine, New York, NY 10016

 # Send all correspondence to:
Sumantra Chatterjee, Ph.D.
Center for Human Genetics & Genomics
New York University Grossman School of Medicine
435 East 30th Street, Room 1012
New York, NY 10016
(212) 263-0233
sumantra.chatterjee@nyulangone.org

Aravinda Chakravarti, Ph.D.
Center for Human Genetics & Genomics
New York University Grossman School of Medicine
435 East 30th Street, Room 802/3
New York, NY 10016
(212) 263-8023
aravinda.chakravarti@nyulangone.org

ORCID IDs:
LEF: 0000-0003-3148-440X
GG: 0009-0002-4842-5238
HBR: 0000-0002-1238-1248
AC: 0000-0002-4264-2285
SC: 0000-0002-5076-1698

Abstract

Hirschsprung disease (HSCR) is a congenital enteric neuropathy caused by disrupted migration, proliferation, and/or differentiation of enteric neural crest-derived cells (ENCDCs), with pathogenic variants at *RET* accounting for a major fraction of cases. While coding variants in *RET* are known to impair enteric nervous system (ENS) development, the causal effects of pathogenic regulatory variants remain poorly understood. The largest contribution to HSCR risk is from a common variant (rs2435357) in an ENS-active, SOX10-bound *RET* enhancer (MCS+9.7) that reduces *RET* gene expression *in vivo* and triggers expression changes in other ENS genes in the human fetal gut. Here, we investigate the role of this enhancer in ENS development using a targeted mouse model by deleting this enhancer (Δmcs9.7). Single-cell RNA-seq profiling of wildtype and Δmcs9.7/ Δmcs9.7 homozygote embryos at the developmental stage E14.5 revealed an ~8% decrease in *Ret* expression within ENS cell clusters, with no gross shifts in ENS cell type composition. *Ret* expression loss was limited to early differentiating neurons and inhibitory motor neurons, indicating cell type-specific enhancer control. To identify the *Ret* functional threshold for normal ENS development, we next generated a compound heterozygous mouse (+/Δmcs9.7; +/CFP), heterozygous null for both the enhancer and coding (CFP) alleles, that showed additive reductions in *Ret* expression in these same cell types and bidirectional feedback between *Ret* and its transcription factor *Sox10*. We observed reduced expression of multiple cell cycle genes and significant loss of nNOS+ and VIP+ neurons in the E14.5 gut, consistent with decreased inhibitory neuron network function driven by loss of proliferation, the hallmark of HSCR. These findings established a cell type-specific role for the mcs9.7 enhancer in modulating *Ret* dosage and revealed how subtle enhancer perturbations alter neural subtype specification without overt aganglionosis. Together, our work uncovers the functional consequences of a common *RET* enhancer variant offering new insights into gene regulatory mechanisms driving HSCR.

Introduction

The enteric nervous system (ENS), the largest component of the peripheral nervous system, is composed of a ganglionic network of over 600 million neurons innervating the entire gastrointestinal (GI) tract (Furness, 2012). This network is formed by the cranio-caudal proliferation, differentiation and migration of Enteric Neural Crest-derived Cells (ENCDCs) in the developing gut across weeks 4 to 8 in the human and embryonic day (E) 10.5 to E14.5 in the mouse embryo (Furness, 2012). One of the key genes involved in this developmental process is the receptor tyrosine kinase *RET* (Natarajan et al., 2002; Uesaka et al., 2008), whose expression in ENCDCs promotes proliferation and cell survival, although the gene is more broadly expressed in other tissues (e.g., kidney, brain, dorsal root ganglia). Significantly, coding and non-coding *RET* deficiency mutations lead to isolated Hirschsprung disease (HSCR) in ~50% of cases, an uncommon (~1/2,500-5,000 live births) developmental disorder of the ENS characterized by the absence of enteric ganglia along variable lengths of the distal bowel (Alves et al., 2013; Tilghman et al., 2019). In the developing mouse gut, *Ret* deficiency leads to significant transcriptional changes affecting numerous transcription factors (TFs), signaling molecules, and specific transport and biosynthesis genes, resulting in aganglionosis (Chatterjee et al., 2019; Heanue and Pachnis, 2006). Analogous genetic changes are observed in the *RET* deficient human fetal gut with HSCR-associated susceptibility alleles in multiple *RET* enhancers (Chatterjee et al., 2023).

The cell type-specific *Ret* loss-of-function (LoF) phenotype has primarily been studied in *Ret* null homozygote mice (Lasrado et al., 2017; Vincent et al., 2023) which demonstrate that complete *Ret* deficiency leads to precocious differentiation and reduction in the number of proliferating ENCDCs leading to these cells' inability to access the inhibitory motor neuron program (Vincent et al., 2023). *Ret* heterozygous mice do not exhibit aganglionosis in the developing gut nor have any other phenotype associated with *Ret* LoF (Kapoor et al., 2017; Vincent et al., 2023). However, *Ret* heterozygote LoF in combination with hypomorphic homozygote mutations in the epistatic endothelin type B receptor gene (*EDNRB*) causes variable aganglionosis (Carrasquillo et al., 2002; McCallion et al., 2003).

In the human, most HSCR patients have heterozygous *RET* variants, some of which are complete LoF but most are hypomorphic; additionally, most patients harbor both *RET* coding and enhancer variants while yet others carry rare and common variants in other ENS and gut mesenchymal genes that are members of a large *RET-EDNRB* gene regulatory network (GRN) (Tilghman et al., 2019). Thus, we hypothesize that the totality of cis and trans sequence variants in an individual that reduce *RET* gene expression to less than 50% of wildtype levels lead to functional *RET* haploinsufficiency and aganglionosis.

To address this hypothesis, we generated mouse models of HSCR with both coding and regulatory *RET* variants. Specifically, we first generated a mouse model by targeting an intronic enhancer of *Ret* (mcs+9.7) whose human homolog is the SOX10-bound *RET* enhancer (MCS+9.7) that harbors a common (24% - 45%) allele that individually increases HSCR risk 4-fold (Emison et al., 2010; Emison et al., 2005). Other *RET* enhancers also harbor polymorphic HSCR-associated variants which can cumulatively increase risk by 10-fold or greater (Chatterjee et al., 2021). Functionally, the common risk allele at MCS+9.7 disrupts SOX10 binding and leads to loss of *RET* function both in neural crest derived neuroblastoma cell lines (Chatterjee et al., 2021) as well as in the human fetal gut (Chatterjee et al., 2023). In addition, we also generated +/Δmcs+9.7; +/CFP compound heterozygote mice by crossing the enhancer disrupted mice with a well characterized *Ret* null heterozygote mouse ($Ret^{+/CFP}$) (Uesaka et al., 2008; Vincent et al., 2023), to study the progressive cellular defects arising from the coding and non-coding *Ret* variants.

To characterize these mice we used single cell (sc) RNA-seq coupled with immunofluorescence of the E14.5 mouse gut. Enhancer deletion homozygotes showed 5% reduction in *Ret* gene expression as well as in other cell type-specific transcriptional changes in the ENS but with no reduction in cell types or numbers. However, double heterozygote mice demonstrated significant reduction (to 42%) in *Ret* gene expression but only in inhibitory motor neurons (iMNs) and a glial cell population expressing progenitor markers. This was accompanied by loss in cell numbers only in the iMNS in the distal hindgut but the glial population was spared. This cell loss is mediated by the reduced proliferative capacity of these cells, providing a mechanistic basic for aganglionosis.

Our studies highlight that the HSCR phenotype results from precise thresholding of *Ret* gene expression below 50% in specific cell types in specific regions of the developing gut. However, HSCR is not a classical haploinsufficiency since the mutant phenotype can arise from more than one mutation affecting the same target gene (*Ret*). These results provide a basis for understanding the genotype-phenotype correlation and HSCR penetrance for different *RET* and other gene mutations in HSCR.

Results

Deletion of a HSCR-associated Ret enhancer in mice leads to loss of Ret expression in vivo

The MCS+9.7 *RET* enhancer, harboring the HSCR-associated common variant rs2435357, is sequence conserved in mice and other vertebrates including the zebrafish (Emison et al., 2005; Grice et al., 2005), and functions as a *RET* enhancer in mouse and zebrafish transgenic assays (Chatterjee et al., 2016; Grice et al., 2005). MCS+9.7 binds SOX10 and regulates the expression of *RET* in human cell lines and the human fetal GI tract (Chatterjee et al., 2023; Chatterjee et al., 2021). First, we assessed the ability of this enhancer to regulate cell-type specific *Ret* expression in the developing mouse gut by deleting a 183 bp segment of the conserved region (Chr6:118,164,102-118,163,917; mm10) centered on the Sox10 binding site within the first intron of *Ret* (**Figure 1A**). We measured gene expression of *Ret* in the developing mouse gut (foregut, caecum, and hind gut) at E12.5 and E14.5, the migratory and proliferative stages of ENS development, using quantitative real time PCR (qRT-PCR). There were no measurable changes in *Ret* expression in heterozygote deleted mice (+/Δmcs+9.7; +/+) at either developmental stage, but a small (5%) yet significant ($p<0.01$) reduction in Δmcs+9.7/Δmcs+9.7; +/+ homozygotes (**Figure 1B**). To determine if the enhancer regulated *Ret* at birth, we measured *Ret* expression at postnatal time 0 (P0) in the small intestine and colon, in the tissues derived from the foregut and hind gut. We detected a similar 5% ($p<0.01$) decrease in *Ret* expression in homozygotes as in development (**Figure 1B**). Thus, the 183bp DNA element is sufficient to act as an *in vivo* developmental enhancer of *Ret* in the gut.

We also generated double heterozygote mice carrying both the Δmcs+9.7 and a *Ret* coding deletion allele by breeding with the *Ret* CFP null mutation (**Methods** (Vincent et al., 2023)), i.e., +/Δmcs+9.7; +/CFP. These latter mice retained, on average, 42% ($p<0.01$) of *Ret* gene expression in the developing gut as compared to the wildtype at both developmental stages and at birth (**Figure 1C**). In previous studies, we demonstrated that reduction of *Ret* gene expression to 50% does not lead to any major transcriptional or cellular changes in the developing GI tract as compared to wildtype embryos (Kapoor et al., 2017; Vincent et al., 2023) but complete *Ret* LoF leads to severe cellular defects and prenatal lethality (Uesaka et al., 2008). Thus, we enquired whether 42%, as opposed to 50%, of *Ret* gene expression altered gut cell composition in any meaningful way. We also ascertained the tissue specificity of this enhancer by measuring gene expression of *Ret* in the developing kidney, an organ whose development is also dependent on the correct spatio-temporal expression of *Ret* (Schuchardt et al., 1994). There are no detectable changes in *Ret* expression in Δmcs+9.7/Δmcs+9.7; +/+embryonic kidneys at either E12.5 or E14.5 but a 50% reduction in +/Δmcs+9.7;+/CFP mice, reflecting the loss of *Ret* gene expression from the heterozygous *Ret* knockout alone with no detectable additional contribution from the deleted enhancer (**Supplementary Figure 1**). Thus mcs+9.7 primarily controls *Ret* expression in the ENCDCs of the developing gut and fate committed ENS cells at birth.

To validate if the observed transcriptional changes in the wildtype, Δmcs+9.7/Δmcs+9.7; +/+, and +/Δmcs+9.7; +/CFP are reflected in the corresponding protein levels *in situ*, we performed immunofluorescence on the whole gut tube for all three genotypes at E14.5. *Ret* gene expression in the migrating ENCDCs was significantly reduced only in +/Δmcs+9.7; +/CFP embryos ($p < 0.01$) as compared to wildtype embryos, leading to loss of migrating ENCDCs in the terminal end of the hindgut near the anal pore (**Figure 1D**). There are no measurable cellular changes in Δmcs+9.7/Δmcs+9.7; +/+mice while *Ret* null (CFP/CFP) mice demonstrated a near complete lack of ENCDCs as previously reported (Vincent et al., 2023). To determine if this cellular effect from reducing *Ret* expression is maintained at birth, we stained the descending colon, the derivate of the hind gut, with Acetylcholinesterase (AChE), the primary cholinergic enzyme found at postsynaptic

neuromuscular junctions, and routinely used as a diagnostic marker for aganglionosis in humans (Yoshimaru et al., 2021) and the mouse (Kapoor et al., 2017; McCallion et al., 2003). We observed significantly reduced cholinergic neuron fibers in the distal colon of +/Δmcs+9.7; +/CFP P0 mice reminiscent of short segment HSCR, with normal innervation observed in wildtype and Δmcs+9.7/Δmcs+9.7; +/+; +/+P0 colons (**Supplementary Figure 2**).

Specific ENS transcriptional and cellular changes from functional loss of a Ret enhancer

We next explored which gut-specific cell type the enhancer was active in. To do so, we performed single cell RNA-seq on dissected gastrointestinal tract (below the stomach to the anal pore) at E14.5, the developmental stage when ENS migration through the gut is complete and ENS cells have started differentiating into neuronal and glial subclasses. We studied tissues from each of two wildtype and Δmcs+9.7/Δmcs+9.7; +/+ homozygote embryos to collect 25,028 wildtype and 35,505 Δmcs+9.7/Δmcs+9.7; +/+ homozygote single cells, respectively (**Methods**). From these data we identified 3,415 high-variability genes and 20 principal components (PCs) to cluster cells based on their differential gene expression (FDR<0.05) across clusters relative to their mean expression in other clusters. Additionally, we used the following as marker genes to specify the identity of each cluster: Smooth muscle (*Acta2, Actg2, Myh11*; 32 % of cells), Epithelial (*Epcam, Cldn7, Lgals4*; 11%), Extra cellular matrix/Fibroblast (*Adamec1, Col6a4, Col3a1*; 30%), Endothelial (*Lars2, Tagln2*; 2%), Immune (*C1qa, C1qb, Cd52*; 2%), ENS (*Ret, Ednrb, Ngfr, Tubb3*; 11%) and a class of undifferentiated but transcriptionally active cells which have yet to acquire any major recognizable cell fate (*H9, Hmga2,Hoxa9*; 11%) (**Figure 2A**). Overall, there is no significant deviation in cell type composition between the wildtype and the Δmcs+9.7/Δmcs+9.7; +/+ GI tracts (p=0.18; hypergeometric test) (**Figure 2B**). This is not surprising given that only 5% of Ret expression is lost in this genotype; note that in heterozygous Ret LoF mice (CFP/+) with 50% loss of Ret expression the phenotype is normal (Vincent et al., 2023).

The ENS is the primary site of action for the Ret mcs+9.7 enhancer. The ENS cells we captured in our single cell experiments comprise 6 major cell types: (1) ENS progenitors

with significantly higher expression (>2-fold; FDR<0.05) of neural crest (NC) markers (e.g., Sox10, Ednrb, Zeb2) as well as glial markers (e.g., Plp1); (2) differentiating neurons and glia expressing pan neuronal and pan glial markers such as Snap25, Plp1, and Mpz, along with dorsal Hox transcription factors like Hoxd5 and Hoxd6; (3) inhibitory motor neurons expressing Nos1 and Vip; (4) excitatory motor neurons expressing Calb2 and Chat; (5) interneurons expressing Scrt1, Nxph4 and Dlx5; and, (6) cholinergic neurons expressing Chat and Slc18a3 (**Figure 2C**). These genes mark a developmental trajectory starting with progenitor cells that lead to more mature neuronal subtypes at the tip of the gene expression manifold with an intermediate state of actively dividing and differentiating neurons. To ascertain if the identified subclusters truly represent a developmental trajectory, we used their gene expression patterns to perform a formal trajectory analysis using Monocle 3 (Trapnell et al., 2014) which tests whether gene expression is associated with pseudo-time. This unsupervised reconstruction analysis does indicate that ENS cells follow the expected developmental path from undifferentiated (placed at time 0) to more mature neuronal cells (**Figure 2D**). Within the ENS cluster, *Ret* expression was reduced by 8% (p<0.001), underscoring the specificity of the mcs+9.7 Ret enhancer (**Figure 2E**). Differential expression analysis of the ENS in wildtype versus Δmcs+9.7/Δmcs+9.7; +/+ mice revealed 174 significantly affected genes (FDR<0.05), of which 51 were neuronal markers. These included the glutamatergic neuronal gene Grin2b (1.67-fold lower, FDR<0.01), interneuron markers Scrt1 and Nxph4 (1.28- and 1.37-fold reductions), and inhibitory motor neuron markers Vip and Nos1 (0.6- and 0.8-fold lower, FDR<0.01 for all) (**Figure 2F**). Comparison with transcriptional profiles from complete Ret-null mouse guts (Vincent et al., 2023) showed that 48 of these 174 genes overlapped with the 520 significantly affected genes (FDR<0.01) in Ret-expressing ENS cells, although the magnitude of change was smaller in the enhancer mutants, consistent with the milder allele (**Supplementary Figure 3**). Notably, these transcriptional changes occurred without detectable alterations in ENS cell composition (**Figure 2B**), indicating that even a modest 5% reduction in Ret expression is sufficient to perturb the same gene regulatory network as in *Ret* null homozygotes, albeit with an attenuated response.

Conversely, 138 genes were significantly upregulated, enriched in two primary processes, regulation of cell size (*Tmod2, Lrp1, Shtn1, Cotl1*) and control of metabolic processes

(*Sgpl1, Idh1, St8sia2*). Among these were also five genes with known roles in neurogenesis (*Mapt, Dcx, Dll3, Islr2, Apoe*). Together, these findings suggest that reduced Ret expression disrupts the transcriptional landscape of the ENS in a bidirectional manner, downregulating key neuronal identity and function genes while upregulating pathways linked to growth, metabolism, and neurogenesis, thereby potentially impairing neuronal development through both loss and gain of transcriptional activity.

Given *Ret*'s role in driving the differentiation of ENCDCs into more mature neuronal fates (Natarajan et al., 2002), our data show that *Ret* expression is nearly absent in progenitor cells at E14.5 but robustly expressed in all other cells (**Figure 2G**). Despite its broad expression in the developing ENS, in Δmcs+9.7/Δmcs+9.7; +/+ homozygotes, expression loss is limited to a 4-fold reduction ($p<0.05$) in differentiating neurons and glia and a 2.3-fold reduction ($p<0.05$) in inhibitory motor neurons compared to wild-type (**Figure 2G**). These results reveal a cell type-specific regulation of *Ret* by the mcs+9.7 enhancer, confined to early differentiating cells and a specific neuronal subtype. Importantly, although enhancer loss affects the transcriptional program in these cells, it does not lead to a detectable cellular phenotype, as identical proportions of cells were found in all clusters in both variant genotypes (**Figure 2H**).

Coding and non-coding Ret variants lead to specific cellular defects in the ENS

A key question in HSCR is how lowering *Ret* gene expression levels below a threshold in the ENS lead to disease penetrance. It is clear that HSCR-associated variants within *RET* enhancers, and other enhancers at *NRG1* and *SEMA3* (Jiang et al., 2015), have lower penetrance than pathogenic *RET* coding variants, with the highest penetrance induced by *RET* null mutations (Tilghman et al., 2019). Indeed, disease segregation (penetrance) in some multiplex HSCR families can be better explained from the combined effects of coding and non-coding mutations at *RET* (Emison et al., 2010), reducing gene expression below a threshold. Therefore, we ascertained the effect of such double heterozygote mutations (+/Δmcs+9.7; +/CFP) on the transcription and cellular architecture of the developing mouse gut. We dissociated cells from GI tracts of two such embryos for a total of 31,244 cells. After stringent quality control (**Methods**), we used 28,181 cells for two-dimensional embedding (UMAP) using 2,000 high-variance genes incorporating 20 PCs. These cells

were classified into the same 7 cell types as previously annotated (**Figure 2A**) and did not show any deviation from expected numbers when compared to either wildtype or the ∆mcs+9.7/∆mcs+9.7; +/+ homozygote (FDR= 0.19; hypergeometric test).

Given that *Ret*'s role during GI development is primarily restricted to the ENS, we therefore assessed 9,760 ENS cells in greater detail from all three genotypes, namely, wildtype (n = 3,752 cells), ∆mcs+9.7/∆mcs+9.7; +/+ (n = 3,183 cells), and +/∆mcs+9.7; +/CFP (n = 2,825 cells). These cells were re-clustered using 1,654 high variance genes and 20 PCs: we obtained eight clusters corresponding to the six major ENS cell types we had detected previously (**Figure 3A**). Combining cells from all 3 genotypes afforded us greater resolution to identify ENS cell subtypes since we could impute missing gene expression from the larger numbers of cells per cluster. The six clusters were annotated based on marker gene expression as Progenitor/Glia: (cluster 0: *Plp1, Mpz*; cluster 1: *Foxd3, Fabp7*; cluster 4: *Mest, S100b),* differentiating neuron and glia (cluster 2: *Cxcl12, Nkain4, Ednrb, Sox10*), inhibitory motor neurons (cluster 3: *Nos1, Vip*), cholinergic neurons (cluster 5: *Slc10a4, Chrnb2*), interneurons (Cluster 6: *Scrt1*, *Dlx5*, *Nxph4*) and excitatory motor neurons (Cluster 7: *Calb2, Chat*). Given our prior section's observation that loss of the mcs9.7 enhancer selectively reduces *Ret* transcription in inhibitory motor neurons (iMNs) and differentiating neurons and glia, we thus asked whether combining enhancer loss with a heterozygous coding deletion (+/Δmcs9.7; +/CFP) would further deplete *Ret* expression in these specific embryonic cell types. Indeed, we observed a 3-fold decrease in *Ret* expression in iMNs and a 2.6-fold decrease in differentiating neurons and glia (FDR < 0.01), underscoring the additive effect of non-coding and coding mutations (**Figure 3B**). All other cell types showed an expected ~50% reduction in *Ret* expression (FDR < 0.01 for all), consistent with a heterozygous coding loss alone. These findings further support a biphasic, cell-type-specific regulation of *Ret* by the mcs9.7 enhancer. We then asked if decreasing *Ret* expression below 50% had any effect on any ENS cell type. Using a chi-squared test for equality of cell proportions, we observed significant depletion of inhibitory motor neurons (39% lower: FDR = $3x10^{-8}$) and differentiating neurons and glia (34% lower: FDR = $2.2x10^{-4}$) in +/∆mcs+9.7; +/CFP embryos as compared to the wildtype; all other clusters has the expected numbers of cells (progenitor cells: p = 0.4, excitatory neurons: p = 0.18, cholinergic neurons: p = 0.3, and interneurons: p = 0.3) (**Figure 3C)**. This cell

depletion is observed in both embryos (replicates) increasing our confidence that this is not an artifact of cell sampling.

Given the increasing evidence pointing to the critical role of iMNs in ENS development (Morarach et al., 2021), and its specific loss attributed to aganglionosis in multiple animal models, including models of *Ret* deficiency (Kuil et al., 2023; Spencer et al., 2021; Vincent et al., 2023), we investigated if cellular loss of this cell type is a direct consequence of loss of *Ret* expression from its lowered enhancer activity. We calculated the proportions of cells which co-expressed both *Ret* and *Sox10*, the transcription factor bound to the mcs+9.7 enhancer, given Sox10's role in regulating genes involved in maintaining progenitor/glial identity (Bondurand and Sham, 2013; Paratore et al., 2002). Note that 88% of Sox10-expressing cells are in the progenitor or differentiating neurons and glia cluster (**Figure 3D**); conversely, 74% of *Ret*-expressing cells are specific lineage-committed neuronal cells of inhibitory (41%), excitatory (16%), cholinergic (12%) and interneurons (5%) (**Figure 3D**), highlighting *Ret*'s role in maintaining overall neuronal identity in the ENS (Natarajan et al., 2002). This analysis revealed, that in inhibitory motor neurons 83% of all cells co-express both genes, but only 18%, 2%, 0.4 % and 0.2% of differentiating neurons and glia, interneurons, excitatory motor neurons and cholinergic neurons, respectively, co-express *Ret* and *Sox10* (**Figure 3D**). We detected no cells co-expressing these genes in progenitor cells (**Figure 3D**). We further assessed *Sox10* expression to investigate potential transcriptional feedback between *Ret* and *Sox10*, as suggested by our earlier tissue-level gene expression studies in the gut. (Chatterjee et al., 2019). We observed a 1.8-fold and 1.6-fold reduction in Sox10 expression in +/Δmcs9.7; +/CFP embryos compared to wildtype (FDR < 0.01 for both), highlighting a cell type–specific positive feedback between *Ret* and its transcription factor *Sox10*. Interestingly, we also detected increased *Sox10* expression in cholinergic neurons in both mutant genotypes relative to wildtype littermates. This upregulation suggests the presence of a previously unrecognized, cell type–specific negative feedback mechanism. Together, these findings reveal a bidirectional regulatory relationship between Ret and Sox10 in the ENS, with distinct effects depending on cellular context. The functional implications of this dual feedback remain to be fully elucidated but point to complex and layered transcriptional interactions between these key regulators.

Since reduced expression of *Ret* dysregulates feedback to *Sox10*, and both are critical drivers of aganglionosis in HSCR (Chatterjee et al., 2016; Chatterjee et al., 2021; Chatterjee et al., 2019), this suggest that iMNs and differentiating neurons and glia, which express both *Ret* and *Sox10*, are the primary cell types affected in HSCR.

Ret deficiency induces specific transcriptional changes in inhibitory motor neurons

Given the significant cellular loss observed in iMNs in +/Δmcs+9.7; +/CFP embryos, we investigated the transcriptional profile of these neurons in greater detail by assessing them separately from the rest of the ENS cells (**Figure 4A**). These cells express the classical iMN markers, *Nos1, Vip, Gal* and *Ntng1*, which have been previously shown to establish the developmental trajectory towards the iMN fate in the ENS by us and others (Morarach et al., 2021; Vincent et al., 2023) (**Figure 4B**). Given the observed cellular loss, we thus measured their gene expression changes and showed that *Nos1, Vip* and *Gal* were reduced by 2.8-fold, 1.6-fold and 1.3-fold (FDR<0.01 for all tests) in +/Δmcs+9.7; +/CFP embryos while *Ntng1* was unaffected (**Figure 4C**). In Δmcs+9.7/Δmcs+9.7; +/+ embryos only *Vip* and *Nos1* were reduced by 0.6 and 0.8-fold (FDR<0.01 for both) but we detected no significant change in expression of either *Gal* or *Ntng1* (**Figure 4C**). We next assessed if this gene expression and cellular loss, observed in our single cell sequencing data, is recapitulated *in vivo*. Thus, we performed immunofluorescence staining for nNOS and Vip in wildtype, Δmcs+9.7/Δmcs+9.7; +/+ and +/Δmcs+9.7; +/CFP embryonic guts at E14.5. While wildtype and Δmcs+9.7/Δmcs+9.7; +/+ embryos demonstrated uninterrupted neuronal connections along the entire length of the gut, both *Nos1* and *Vip* positive neurons were significantly reduced at the distal end of the hindgut near the future anal pore in +/Δmcs+9.7; +/CFP embryos (**Figure 4D**). Additionally, while *Nos1* positive neurons, though reduced in numbers, were present with near normal morphology, *Vip* positive neurons were clustered together in the distal hindgut (**Figure 4D**), a hallmark of loss of proliferative and migratory capacity. This latter feature has been previously observed in surviving ENCDCs of *Ret* null embryos (Hirst et al., 2017; Vincent et al., 2023). Measurement of fluorescence intensity for neuronal markers (nNOS, VIP) revealed a 10-fold reduction in nNOS-positive neurons and a 5-fold reduction in VIP-expressing neurons

in the hindgut of +/Δmcs9.7; +/CFP embryos compared to wildtype controls (**Figure 4D**), indicating a substantial loss of inhibitory motor neurons in the compound mutants.

iMN specific effect in the HSCR specific GRN

Despite significant genetic heterogeneity, ~67% of HSCR patients have mutations in genes of the *RET-EDNRB* gene regulatory network (GRN) (Tilghman et al., 2019). This GRN specifies bidirectional transcriptional feedback between *RET* and *EDNRB*, their transcription factors *SOX10, GATA2, RARB,* and *NKX2-5,* the *RET* co-receptor *GFRA1*, their ligands *GDNF* and *EDN3*, and the phosphorylated RET ubiquitin ligase degrader *CBL* (Chatterjee and Chakravarti, 2019). To ascertain whether this feedback is associated with the iMN phenotype we observed, we quantified the expression of these genes and their changes in *Ret* deficiency. There is no expression of *Gdnf* and *Edn3* in iMN cells, as expected, since they are expressed and secreted from the surrounding mesenchyme (Baynash et al., 1994; Natarajan et al., 2002). *Ret* and its co-receptor *Gfra1* are downregulated 8-fold and 1.3-fold, respectively, while *Ednrb* is downregulated 6.2-fold (FDR<0.01 for all) in iMNs of +/Δmcs+9.7; +/CFP mice as compared to the wildtype (**Figure 5A**). Only *Ret* is significantly (FDR<0.01) downregulated in the Δmcs+9.7/Δmcs+9.7; +/+ gut by 1.28-fold leaving both *Gfra1* and *Ednrb* unaffected. Among the transcription factors controlling *Ret* and *Ednrb*, we did not observe expression of *Gata2* and *Nkx2-5* in iMN cells at E14.5 but *Sox10* is reduced by 12-fold and 6-fold (FDR<0.01 for both), respectively, in +/Δmcs+9.7; +/CFP and Δmcs+9.7/Δmcs+9.7; +/+ iMN cells, respectively. Thus, both the small 5% and the large 58% loss of *Ret* expression has transcriptional changes affecting the same core GRN disrupted in HSCR leading to observable cellular changes in inhibitory motor neurons. In light of our results, it is unsurprising that the developmental trajectory leading to iMN formation is completely lost in *Ret* null embryos, as we have previously shown (Vincent et al., 2023).

Ret deficiency decreases proliferative capacity in iMNs

Reduction in proliferation capacity due to complete LoF of genes within the developing ENS, particularly those within the *Ret-Ednrb* GRN, are significant drivers of aganglionosis in the gut (Bergeron et al., 2016; Fujiwara et al., 2018; Vincent et al., 2023). Therefore, we

asked whether similar but attenuated mechanisms operate to explain the iMN changes in +/Δmcs+9.7; +/ CFP embryos. Differential gene expression analysis at E14.5 with respect to both genotype and cell type identified 93 (48 upregulated and 45 downregulated) genes that are significantly (FDR<0.05) differentially expressed in the iMNs of +/Δmcs+9.7; +/ CFP embryos, as compared to their wildtype littermates (**Figure 5B, Supplementary table 1**). These include 10 genes involved in the cell cycle, 8 of which (*Ccnb2, Ccnb1, Ccna2, Cenpf, Cenpe, Cenpk,Top2a, Cdk1*) are >1.6-fold downregulated (FDR<0.01 for all) and *Cdkn1c* and *Ccnd1*, which are 0.8- and 0.6-fold upregulated (FDR<0.01 for both), respectively (**Figure 5B**). Genes involved in DNA replication (*Gmnn, Mcm3, Mcm6, Mcm5, Mcm1*) and regulation of the cell cycle (*Rdcc, Mad2l1, Chek2, Rad51ap1*) were also downregulated between 1.4-fold and 2-fold (FDR<0.01 for all) (**Figure 5C and Supplementary table 2**). In Δmcs+9.7/Δmcs+9.7; +/+ embryos all these 19 genes show a similar direction of change when compared to wildtype littermates but not all are statistically significant. Thus, both cell cycle occupancy and differentiation state, processes linked to proliferation, are disrupted in the double heterozygote as compared to wildtype embryos, specially affecting both a glial population with progenitor markers and iMNs. In our mouse models we show that the observed gene expression changes and the subsequent cellular losses are restricted to the hindgut, modeling short segment HSCR. To validate this predicted decreased proliferation in +/Δmcs+9.7: +/CFP iMNs, we thus used immuno-fluorescence to assess the number of nNOS positive cells co-expressing the mitotic marker phosphohistone H3 (pH3) within the developing gut at E14.5 (**Figure 5D**). We confirmed a 54% (Student's *t* test, $p < 10^{-4}$) overall reduction in the number of nNOS+/pH3+ neurons only in the hind gut in the Δmcs+9.7,+/CFP mouse model consistent with the reduced expression of key cell cycle regulators, highlighting the loss of iMNs is indeed driven by loss of proliferation in these cells, as we previously showed for the whole ENS (Vincent et al., 2023).

Discussion

Numerous genomic studies of complex disorders have implicated both rare coding and common noncoding variants as causal genetic factors for their etiology (Chatterjee et al., 2016; Kapoor et al., 2014; Kelly et al., 2022). However, it remains unclear how noncoding

variants with small-to-modest genetic effects impact the same *phenotype* as their cognate large-effect coding variants. The latter are assumed to affect a rate-limiting gene's function critically and therefore lead to a phenotype directly. But how do noncoding variants affect the same phenotype when the genomic evidence suggests that many such variants are required? We have previously hypothesized that this occurs only when the cumulative effect of all variants affect the same rate limiting step (a protein or a process modulated by several proteins) as the major coding mutations (Chakravarti and Turner, 2016). We now provide evidence that, at least for HSCR, quantitative changes in *Ret* gene expression from both coding and noncoding variants, and its protein, affect the same gut developmental process in the same cells in the ENS at the same developmental time but do not affect all the target genes. The HSCR pathology (aganglionosis) results only when all target genes are affected as occurs through major qualitative changes in *Ret* gene expression and its protein.

The research described here provides some clues as to why these two genetic architectures, coding and noncoding, have different quantitative properties: higher vs lower penetrance; lower vs higher phenotypic variability. Despite affecting the same gut developmental program and the same GRN of genes, noncoding and coding *Ret* variants induce attenuated versus amplified responses of inhibitory motor neurons and a glial population with progenitor markers. Although such changes are now detectable at the single cell gene expression level, coding variants leads to phenotypic penetrance frequently while noncoding variants do so rarely. Why? A primary cause for this difference may be the stochastic nature of cell differentiation and proliferation, and *how many* cells are affected. Note that most but not all *RET* null heterozygotes have 100% penetrance (Emison et al., 2010). Thus, we believe that the number of cells which are affected, assumed to be those which have less than the optimum *Ret* gene expression of 50%, is larger in major coding mutations than in the common non-coding variants. Occasionally, the optimum is breached even with non-coding variants but this occurs rarely (lower penetrance).

Our results also demonstrate that the 'aganglionosis' detected in human patients, and currently tested for in mouse models, from acetylcholinesterase staining, might arise from

loss of *specific cell types* and is not a broad loss of all neuronal cells, as previously thought (Furness, 2012). This increases the stochasticity of penetrance because smaller numbers of cells are at risk increasing the role of functional 'drift.' Thus, pathophysiological studies of HSCR might benefit from the use of additional histopathological markers to assess the phenotype in patients. This comment pertains to both the aganglionic, hypoganglionic and transition zone segments of the gut.

One of the yet unsolved questions in HSCR is why do the lengths of aganglionic bowel (colon) differ in different patients, and why is short segment disease the most common (Badner et al., 1990)? Although heritable, many families have mixed short and long segment disease: the genetic basis of this segment length variation remains unclear but at least in some families arises from the interaction between *Ret* coding and enhancer variants (Emison et al., 2010; Emison et al., 2005). Previously studied mouse models have either total intestinal aganglionosis from complete *Ret* deficiency (Uesaka et al., 2008), which is extremely rare in humans, or variable long segment disease from multigenic models (Hirst et al., 2017; McCallion et al., 2003). Our double heterozygote mouse model with 42% *Ret* gene expression presents with aganglionosis only in the distal hindgut, thus most closely modeling short segment HSCR, the most common phenotype.

Finally, our data reaffirms previous observations that aganglionosis in HSCR animal models arises from proliferative defects in cells of the ENS. But why do all the cellular changes in these models affect only iMNs (Kuil et al., 2023; Spencer et al., 2021; Vincent et al., 2023)? One possible answer is that HSCR is basically a proliferative defect of iMNs and not a broad aganglionosis as previously assumed (Furness, 2012). But suspicion remains that the human cellular phenotype may be more complex than in the mouse, since recent studies of ENCDCs derived from HSCR patient-induced pluripotent stem cells shows that both gene expression and cell type composition are different from mouse ENCDCs, with both committed glial progenitors (GP) and the neuronal progenitors (NP) absent in patient-derived ENCDCs; this feature has not been recapitulated in mouse models (Li et al., 2023). Given the limited sample size and technical variations in deriving ENCDCs this observed difference needs to yet be conclusively proven. To investigate these contrasting

hypotheses directly, mouse models with human *RET* coding and noncoding normal and disease-associated haplotypes are indispensable.

Materials and Methods

Nomenclature of mutant mice

Our mouse models include disruptions in both the coding and enhancer regions of the same gene, an approach not commonly used in human genetic studies. To ensure clarity, as well as correspondence between the human and mouse orthologous elements, we provide the nomenclature table below, which we have consistently applied throughout the manuscript.

***Ret* enhancer genotype**	***Ret* coding genotype**	**Genotype of mouse strain**
+/+	+/+	+/+; +/+ or Wildtype (WT)
+/deletion	+/+	+/Δmcs+9.7; +/+
deletion/deletion	+/+	Δmcs+9.7/Δmcs+9.7; +/+
+/deletion	+/deletion	+/Δmcs+9.7; +/CFP

Generation of Ret deficient mouse models

mcs+9.7 deletion mice: We used the following guide RNAs to delete the *RET* enhancer MCS+9.7 (chr10: 43,581,812–43,582,711; hg19) conserved in mice (mcs+9.7: 6:118,164,102-118,163,917; mmu39) with sequence identity 88%: Forward Guide: TCCTTCCGGCTTCTAGACAA (chr 6:118163913 – 118163932) and Reverse Guide: GCAGCAGCAACAGCTACTTG (chr 6:118164067 – 118164086). The guides were designed to delete a DNA fragment within the conserved sequence centered on the known Sox10 binding site. They were injected with Cas9 protein into one cell embryos by standard methods at the NYU transgenic core facility to delete the target DNA segment. We used the following primers to routinely genotype these mice: mcs+9.7 mKO-F: CACGTCCTGTCTCTTCCGTAG and mcs+9.7 mKO-R: AGCCTGTGAACGTGTTCTGC. Both the heterozygous and homozygous mcs+9.7 deletion (Δ) mice were born in the expected Mendelian proportions (**Supplementary Table 3-6**). These are referred to as Δmcs+9.7/+; +/+ and Δmcs+9.7/Δmcs+9.7; +/+, respectively.

***Ret* CFP knock-in mice (*Ret*$^{CFP/+}$; MGI:3777556):** These mice were generated by crossing *Ret*fl/+ mice to β-actin-Cre mice to remove the RET9 cDNA: these mice were maintained on a C57BL/6 background and have been previously described in detail (Vincent et al., 2023). To generate double heterozygote mice deleted for both the mcs+9.7 enhancer and the coding sequence of *Ret*, +/Δmcs+9.7; +/+ mice were crossed to +/+; *CFP/*+ mice to produce Δmcs+9.7/Δmcs+9.7; +/+ and +/Δmcs+9.7; +/CFP genotypes (the mutant sites are listed as mcs+9.7 and coding, respectively); all offspring were in expected Mendelian proportions (Supplementary Table 1). All mouse experiments were conducted in accordance with the NIH Guidance for the Care and Use of Laboratory Animals. All procedures were approved by the NYU School of Medicine Animal Care and Use Committee (Protocol number: s17-01779).

Dissection and dissociation of embryonic tissue

Foregut and hindgut tissue from Δmcs+9.7/Δmcs+9.7; +/+ and Δmcs+9.7/Δmcs+9.7; +/CFP embryos at E12.5 and E14.5 were dissociated into single-cell suspensions using Accumax (Sigma, USA). The cells were filtered serially through a 100 μm and 40 μm cell strainer, and centrifuged at 2,000 rpm for 5 m. The cell pellets were resuspended in 5% FBS, 4 mM EDTA in Leibovitz L-15 medium. This cell suspension was diluted to 20,000 cells and processed through the 10X Genomics GEM generator to create a standard 3' library using the 10X Genomics standard protocol. These cells were sequenced at an average of $1x10^5 \pm 10^4$ reads/cell.

Single cell gene expression (RNA-seq) analysis

Sequence files were processed through *CellRanger* to generate the *barcodes, features* and *matrix* files. These files were processed through *Seurat* (Stuart et al. 2019) to generate a matrix count file. Individual datasets for each genotype were then analyzed by normalizing and scaling the data followed by detecting highly variable genes across cell types for downstream analysis using *sctransform* in *Seurat* (Hafemeister et al. 2019). Cells which met the following criteria were retained for further downstream analysis: (nUMI >= 500) & (nGene >= 250) & (log10GenesPerUMI > 0.80) and (mitoRatio < 0.20)). We only retained those genes which were detected in >10 cells. To eliminate technical differences between datasets and to perform comparative scRNA-seq analysis across experimental conditions

we utilized *Integration* analysis in *Seurat* which matched shared cell populations across datasets. To avoid bias, these methods first identified cross-dataset pairs of cells that were in a matched biological state ('anchors') before creating clusters. These were used as input to the uniform manifold approximation and projection (UMAP) dimensionality reduction tool to establish a biologically relevant two-dimensional embedding of the cells. All raw and processed single cell data files are available at Gene Expression Omnibus (GEO) under accession number GSE304252. The analysis pipeline used for *Seurat* can be found at https://github.com/SumantraChatt/mouse-scRNAseq/tree/main

Single cell differential gene expression analysis

We used Seurat's *FindMarker* feature to perform differential expression by pseudo-bulking the samples either across genotypes or across cell clusters. We utilized "MAST": GLM-framework (Finak et al., 2015) that treated the cellular detection rate as a covariate within *Seurat*.

Cell-type annotation

We annotated cell types by differential gene expression analysis by considering all markers with >1.5-fold change (FDR<0.05) in that cluster as compared to all other clusters. These genes were analyzed for their GO terms using DAVID (Huang et al., 2007) and enriched GO terms (FDR <0.01 and containing >10 genes) were used to annotate the clusters. Additionally, we used *clusterprofiler* (v 4.16.0) (Yu et al., 2012) to annotate genes into biological processes from both the GO and Kyoto Encyclopedia of Genes and Genomes (KEGG) pathways for confirmation of the primary annotation using DAVID. For the enteric nervous system cluster, along with using unbiased cell type marker identification we also used previously published markers for specific neuronal and glial cell types in the ENS (Elmentaite et al., 2021; Morarach et al., 2021; Vincent et al., 2023).

Immunofluorescence assays on whole mouse gut

Whole gut tissues, at E12.5 and E14.5 were dissected and washed in ice-cold PBS followed by fixation in 4% PFA at 4°C for 1 h. The fixed tissues were permeabilized and blocked with 5% normal donkey serum and 0.3% Triton-X for 1 h at room temperature (RT). The tissues were incubated with appropriate primary antibodies at 4°C overnight, washed

with PBS, then incubated in appropriate secondary antibodies at 4°C overnight (see Supplementary table 7 for antibodies and dilutions). Tissues were washed in PBS and incubated with 0.2 µg/mL of DAPI (4′,6-diamidino-2-phenylindole) for 10 m at RT, followed by incubation for 20 m at RT with CUBIC-1 (16) diluted 1:10 with PBS.
Samples were washed with PBS and mounted on Fisherbrand Superfrost Plus microscope slides with ProLong Gold Antifade mounting media and imaged using a Zeiss AxioVert Microscope.

Image Analysis

The following workflow was used in ImageJ to analyze fluorescent images, using previously described methods for neuronal density (Berk-Rauch et al., 2023). Fluorescence intensity of specific markers (nNOS, VIP, RET) were used as a proxy for neuronal density within each hindgut region. For each image, the area positive for marker staining was quantified and expressed as a percentage of the total area of the region of interest. Genotype information was blinded to the observer during analysis. Data are presented as mean marker intensity across the region of interest from multiple biological replicates per genotype. For double fluorescence analysis (nNOS and pH3), the intensity of each fluorescent marker was quantified in ImageJ. Regions where both markers co-localized within the same cell were identified and used for further analysis. Data are presented as the average intensity of each marker within co-expressing regions across the entire distal colon, averaged over multiple embryos per genotype. Statistical significance was assessed using a paired Student's *t*-test.

Author Contributions

SC and AC conceived and designed the study. LEF and HRB created all mouse constructs. LEF,GG, LW conducted single cell and immunofluorescence assays; SC and LEF analyzed the data. SC and AC wrote the manuscript. All authors approved the final version of the manuscript.

Declaration of Interests

The authors declare no competing interests.

Acknowledgement

This work was supported by NIH grants DK135089 to AC and SC, HD116004 to SC, and HD028088 to AC. The funders had no role in design of the study or data interpretation.

References

Alves, M.M., Sribudiani, Y., Brouwer, R.W., Amiel, J., Antinolo, G., Borrego, S., Ceccherini, I., Chakravarti, A., Fernandez, R.M., Garcia-Barcelo, M.M., Griseri, P., Lyonnet, S., Tam, P.K., van Ijcken, W.F., Eggen, B.J., te Meerman, G.J., Hofstra, R.M., 2013. Contribution of rare and common variants determine complex diseases-Hirschsprung disease as a model. Dev Biol 382, 320-329.

Badner, J.A., Sieber, W.K., Garver, K.L., Chakravarti, A., 1990. A genetic study of Hirschsprung disease. Am J Hum Genet 46, 568-580.

Baynash, A.G., Hosoda, K., Giaid, A., Richardson, J.A., Emoto, N., Hammer, R.E., Yanagisawa, M., 1994. Interaction of endothelin-3 with endothelin-B receptor is essential for development of epidermal melanocytes and enteric neurons. Cell 79, 1277-1285.

Bergeron, K.F., Nguyen, C.M., Cardinal, T., Charrier, B., Silversides, D.W., Pilon, N., 2016. Upregulation of the Nr2f1-A830082K12Rik gene pair in murine neural crest cells results in a complex phenotype reminiscent of Waardenburg syndrome type 4. Dis Model Mech 9, 1283-1293.

Berk-Rauch, H.E., Choudhury, A., Richards, A.T., Singh, P.K., Chen, Z.L., Norris, E.H., Strickland, S., Ahn, H.J., 2023. Striatal fibrinogen extravasation and vascular degeneration correlate with motor dysfunction in an aging mouse model of Alzheimer's disease. Front Aging Neurosci 15, 1064178.

Bondurand, N., Sham, M.H., 2013. The role of SOX10 during enteric nervous system development. Dev Biol 382, 330-343.

Carrasquillo, M.M., McCallion, A.S., Puffenberger, E.G., Kashuk, C.S., Nouri, N., Chakravarti, A., 2002. Genome-wide association study and mouse model identify interaction between RET and EDNRB pathways in Hirschsprung disease. Nat Genet 32, 237-244.

Chakravarti, A., Turner, T.N., 2016. Revealing rate-limiting steps in complex disease biology: The crucial importance of studying rare, extreme-phenotype families. Bioessays 38, 578-586.

Chatterjee, S., Chakravarti, A., 2019. A gene regulatory network explains RET-EDNRB epistasis in Hirschsprung disease. Hum Mol Genet 28, 3137-3147.

Chatterjee, S., Fries, L.E., Yaacov, O., Hu, N., Berk-Rauch, H.E., Chakravarti, A., 2023. RET enhancer haplotype-dependent remodeling of the human fetal gut development program. PLoS Genet 19, e1011030.

Chatterjee, S., Kapoor, A., Akiyama, J.A., Auer, D.R., Lee, D., Gabriel, S., Berrios, C., Pennacchio, L.A., Chakravarti, A., 2016. Enhancer Variants Synergistically Drive

Dysfunction of a Gene Regulatory Network In Hirschsprung Disease. Cell 167, 355-368 e310.

Chatterjee, S., Karasaki, K.M., Fries, L.E., Kapoor, A., Chakravarti, A., 2021. A multi-enhancer RET regulatory code is disrupted in Hirschsprung disease. Genome Res 31, 2199-2208.

Chatterjee, S., Nandakumar, P., Auer, D.R., Gabriel, S.B., Chakravarti, A., 2019. Gene- and tissue-level interactions in normal gastrointestinal development and Hirschsprung disease. Proc Natl Acad Sci U S A 116, 26697-26708.

Elmentaite, R., Kumasaka, N., Roberts, K., Fleming, A., Dann, E., King, H.W., Kleshchevnikov, V., Dabrowska, M., Pritchard, S., Bolt, L., Vieira, S.F., Mamanova, L., Huang, N., Perrone, F., Goh Kai'En, I., Lisgo, S.N., Katan, M., Leonard, S., Oliver, T.R.W., Hook, C.E., Nayak, K., Campos, L.S., Dominguez Conde, C., Stephenson, E., Engelbert, J., Botting, R.A., Polanski, K., van Dongen, S., Patel, M., Morgan, M.D., Marioni, J.C., Bayraktar, O.A., Meyer, K.B., He, X., Barker, R.A., Uhlig, H.H., Mahbubani, K.T., Saeb-Parsy, K., Zilbauer, M., Clatworthy, M.R., Haniffa, M., James, K.R., Teichmann, S.A., 2021. Cells of the human intestinal tract mapped across space and time. Nature 597, 250-255.

Emison, E.S., Garcia-Barcelo, M., Grice, E.A., Lantieri, F., Amiel, J., Burzynski, G., Fernandez, R.M., Hao, L., Kashuk, C., West, K., Miao, X., Tam, P.K., Griseri, P., Ceccherini, I., Pelet, A., Jannot, A.S., de Pontual, L., Henrion-Caude, A., Lyonnet, S., Verheij, J.B., Hofstra, R.M., Antinolo, G., Borrego, S., McCallion, A.S., Chakravarti, A., 2010. Differential contributions of rare and common, coding and noncoding Ret mutations to multifactorial Hirschsprung disease liability. Am J Hum Genet 87, 60-74.

Emison, E.S., McCallion, A.S., Kashuk, C.S., Bush, R.T., Grice, E., Lin, S., Portnoy, M.E., Cutler, D.J., Green, E.D., Chakravarti, A., 2005. A common sex-dependent mutation in a RET enhancer underlies Hirschsprung disease risk. Nature 434, 857-863.

Finak, G., McDavid, A., Yajima, M., Deng, J., Gersuk, V., Shalek, A.K., Slichter, C.K., Miller, H.W., McElrath, M.J., Prlic, M., Linsley, P.S., Gottardo, R., 2015. MAST: a flexible statistical framework for assessing transcriptional changes and characterizing heterogeneity in single-cell RNA sequencing data. Genome Biol 16, 278.

Fujiwara, N., Nakazawa-Tanaka, N., Miyahara, K., Arikawa-Hirasawa, E., Akazawa, C., Yamataka, A., 2018. Altered expression of laminin alpha1 in aganglionic colon of endothelin receptor-B null mouse model of Hirschsprung's disease. Pediatr Surg Int 34, 137-141.

Furness, J.B., 2012. The enteric nervous system and neurogastroenterology. Nat Rev Gastroenterol Hepatol 9, 286-294.

Grice, E.A., Rochelle, E.S., Green, E.D., Chakravarti, A., McCallion, A.S., 2005. Evaluation of the RET regulatory landscape reveals the biological relevance of a HSCR-implicated enhancer. Hum Mol Genet 14, 3837-3845.

Heanue, T.A., Pachnis, V., 2006. Expression profiling the developing mammalian enteric nervous system identifies marker and candidate Hirschsprung disease genes. Proc Natl Acad Sci U S A 103, 6919-6924.

Hirst, C.S., Stamp, L.A., Bergner, A.J., Hao, M.M., Tran, M.X., Morgan, J.M., Dutschmann, M., Allen, A.M., Paxinos, G., Furlong, T.M., McKeown, S.J., Young, H.M., 2017. Kif1bp loss in mice leads to defects in the peripheral and central nervous system and perinatal death. Sci Rep 7, 16676.

Huang, D.W., Sherman, B.T., Tan, Q., Collins, J.R., Alvord, W.G., Roayaei, J., Stephens, R., Baseler, M.W., Lane, H.C., Lempicki, R.A., 2007. The DAVID Gene Functional Classification Tool: a novel biological module-centric algorithm to functionally analyze large gene lists. Genome Biol 8, R183.

Jiang, Q., Arnold, S., Heanue, T., Kilambi, K.P., Doan, B., Kapoor, A., Ling, A.Y., Sosa, M.X., Guy, M., Jiang, Q., Burzynski, G., West, K., Bessling, S., Griseri, P., Amiel, J., Fernandez, R.M., Verheij, J.B., Hofstra, R.M., Borrego, S., Lyonnet, S., Ceccherini, I., Gray, J.J., Pachnis, V., McCallion, A.S., Chakravarti, A., 2015. Functional loss of semaphorin 3C and/or semaphorin 3D and their epistatic interaction with ret are critical to Hirschsprung disease liability. Am J Hum Genet 96, 581-596.

Kapoor, A., Auer, D.R., Lee, D., Chatterjee, S., Chakravarti, A., 2017. Testing the Ret and Sema3d genetic interaction in mouse enteric nervous system development. Hum Mol Genet 26, 1811-1820.

Kapoor, A., Sekar, R.B., Hansen, N.F., Fox-Talbot, K., Morley, M., Pihur, V., Chatterjee, S., Brandimarto, J., Moravec, C.S., Pulit, S.L., Consortium, Q.T.I.-I.G., Pfeufer, A., Mullikin, J., Ross, M., Green, E.D., Bentley, D., Newton-Cheh, C., Boerwinkle, E., Tomaselli, G.F., Cappola, T.P., Arking, D.E., Halushka, M.K., Chakravarti, A., 2014. An enhancer polymorphism at the cardiomyocyte intercalated disc protein NOS1AP locus is a major regulator of the QT interval. Am J Hum Genet 94, 854-869.

Kelly, T.N., Sun, X., He, K.Y., Brown, M.R., Taliun, S.A.G., Hellwege, J.N., Irvin, M.R., Mi, X., Brody, J.A., Franceschini, N., Guo, X., Hwang, S.J., de Vries, P.S., Gao, Y., Moscati, A., Nadkarni, G.N., Yanek, L.R., Elfassy, T., Smith, J.A., Chung, R.H., Beitelshees, A.L., Patki, A., Aslibekyan, S., Blobner, B.M., Peralta, J.M., Assimes, T.L., Palmas, W.R., Liu, C., Bress, A.P., Huang, Z., Becker, L.C., Hwa, C.M., O'Connell, J.R., Carlson, J.C., Warren, H.R., Das, S., Giri, A., Martin, L.W., Craig Johnson, W., Fox, E.R., Bottinger, E.P., Razavi, A.C., Vaidya, D., Chuang, L.M., Chang, Y.C., Naseri, T., Jain, D., Kang, H.M., Hung, A.M., Srinivasasainagendra, V., Snively, B.M., Gu, D., Montasser, M.E., Reupena, M.S., Heavner, B.D., LeFaive, J., Hixson, J.E., Rice, K.M., Wang, F.F., Nielsen, J.B., Huang, J., Khan, A.T., Zhou, W., Nierenberg, J.L., Laurie, C.C., Armstrong, N.D., Shi, M., Pan, Y., Stilp, A.M., Emery, L., Wong, Q., Hawley, N.L., Minster, R.L., Curran, J.E., Munroe, P.B., Weeks, D.E., North, K.E., Tracy, R.P., Kenny, E.E., Shimbo, D., Chakravarti, A., Rich, S.S., Reiner, A.P., Blangero, J., Redline, S., Mitchell, B.D., Rao, D.C., Ida Chen, Y.D., Kardia, S.L.R., Kaplan, R.C., Mathias, R.A., He, J., Psaty, B.M., Fornage, M., Loos, R.J.F., Correa, A., Boerwinkle, E., Rotter, J.I.,

Kooperberg, C., Edwards, T.L., Abecasis, G.R., Zhu, X., Levy, D., Arnett, D.K., Morrison, A.C., Samoan Obesity, L., Genetic Adaptations Study Group, d.d.N.T.-O.f.P.M.T.C., 2022. Insights From a Large-Scale Whole-Genome Sequencing Study of Systolic Blood Pressure, Diastolic Blood Pressure, and Hypertension. Hypertension 79, 1656-1667.

Kuil, L.E., Kakiailatu, N.J.M., Windster, J.D., Bindels, E., Zink, J.T.M., van der Zee, G., Hofstra, R.M.W., Shepherd, I.T., Melotte, V., Alves, M.M., 2023. Unbiased characterization of the larval zebrafish enteric nervous system at a single cell transcriptomic level. iScience 26, 107070.

Lasrado, R., Boesmans, W., Kleinjung, J., Pin, C., Bell, D., Bhaw, L., McCallum, S., Zong, H., Luo, L., Clevers, H., Vanden Berghe, P., Pachnis, V., 2017. Lineage-dependent spatial and functional organization of the mammalian enteric nervous system. Science 356, 722-726.

Li, Z., Lui, K.N., Lau, S.T., Lai, F.P., Li, P., Chung, P.H., Wong, K.K., Tam, P.K., Garica-Barcelo, M.M., Hui, C.C., Sham, P.C., Ngan, E.S., 2023. Transcriptomics of Hirschsprung disease patient-derived enteric neural crest cells reveals a role for oxidative phosphorylation. Nat Commun 14, 2157.

McCallion, A.S., Stames, E., Conlon, R.A., Chakravarti, A., 2003. Phenotype variation in two-locus mouse models of Hirschsprung disease: tissue-specific interaction between Ret and Ednrb. Proc Natl Acad Sci U S A 100, 1826-1831.

Morarach, K., Mikhailova, A., Knoflach, V., Memic, F., Kumar, R., Li, W., Ernfors, P., Marklund, U., 2021. Diversification of molecularly defined myenteric neuron classes revealed by single-cell RNA sequencing. Nat Neurosci 24, 34-46.

Natarajan, D., Marcos-Gutierrez, C., Pachnis, V., de Graaff, E., 2002. Requirement of signalling by receptor tyrosine kinase RET for the directed migration of enteric nervous system progenitor cells during mammalian embryogenesis. Development 129, 5151-5160.

Paratore, C., Eichenberger, C., Suter, U., Sommer, L., 2002. Sox10 haploinsufficiency affects maintenance of progenitor cells in a mouse model of Hirschsprung disease. Hum Mol Genet 11, 3075-3085.

Schuchardt, A., D'Agati, V., Larsson-Blomberg, L., Costantini, F., Pachnis, V., 1994. Defects in the kidney and enteric nervous system of mice lacking the tyrosine kinase receptor Ret. Nature 367, 380-383.

Spencer, N.J., Travis, L., Wiklendt, L., Costa, M., Hibberd, T.J., Brookes, S.J., Dinning, P., Hu, H., Wattchow, D.A., Sorensen, J., 2021. Long range synchronization within the enteric nervous system underlies propulsion along the large intestine in mice. Commun Biol 4, 955.

Tilghman, J.M., Ling, A.Y., Turner, T.N., Sosa, M.X., Krumm, N., Chatterjee, S., Kapoor, A., Coe, B.P., Nguyen, K.H., Gupta, N., Gabriel, S., Eichler, E.E., Berrios, C., Chakravarti, A., 2019. Molecular Genetic Anatomy and Risk Profile of Hirschsprung's Disease. N Engl J Med 380, 1421-1432.

Trapnell, C., Cacchiarelli, D., Grimsby, J., Pokharel, P., Li, S., Morse, M., Lennon, N.J., Livak, K.J., Mikkelsen, T.S., Rinn, J.L., 2014. The dynamics and regulators of cell fate decisions are revealed by pseudotemporal ordering of single cells. Nat Biotechnol 32, 381-386.

Uesaka, T., Nagashimada, M., Yonemura, S., Enomoto, H., 2008. Diminished Ret expression compromises neuronal survival in the colon and causes intestinal aganglionosis in mice. J Clin Invest 118, 1890-1898.

Vincent, E., Chatterjee, S., Cannon, G.H., Auer, D., Ross, H., Chakravarti, A., Goff, L.A., 2023. Ret deficiency decreases neural crest progenitor proliferation and restricts fate potential during enteric nervous system development. Proc Natl Acad Sci U S A 120, e2211986120.

Yoshimaru, K., Matsuura, T., Yanagi, Y., Obata, S., Takahashi, Y., Kajihara, K., Ohmori, A., Irie, K., Hino, Y., Shibui, Y., Tamaki, A., Kohashi, K., Oda, Y., Taguchi, T., 2021. Reevaluation of concurrent acetylcholinesterase and hematoxylin and eosin staining for Hirschsprung's disease. Pediatr Int 63, 1095-1102.

Yu, G., Wang, L.G., Han, Y., He, Q.Y., 2012. clusterProfiler: an R package for comparing biological themes among gene clusters. OMICS 16, 284-287.

Figures

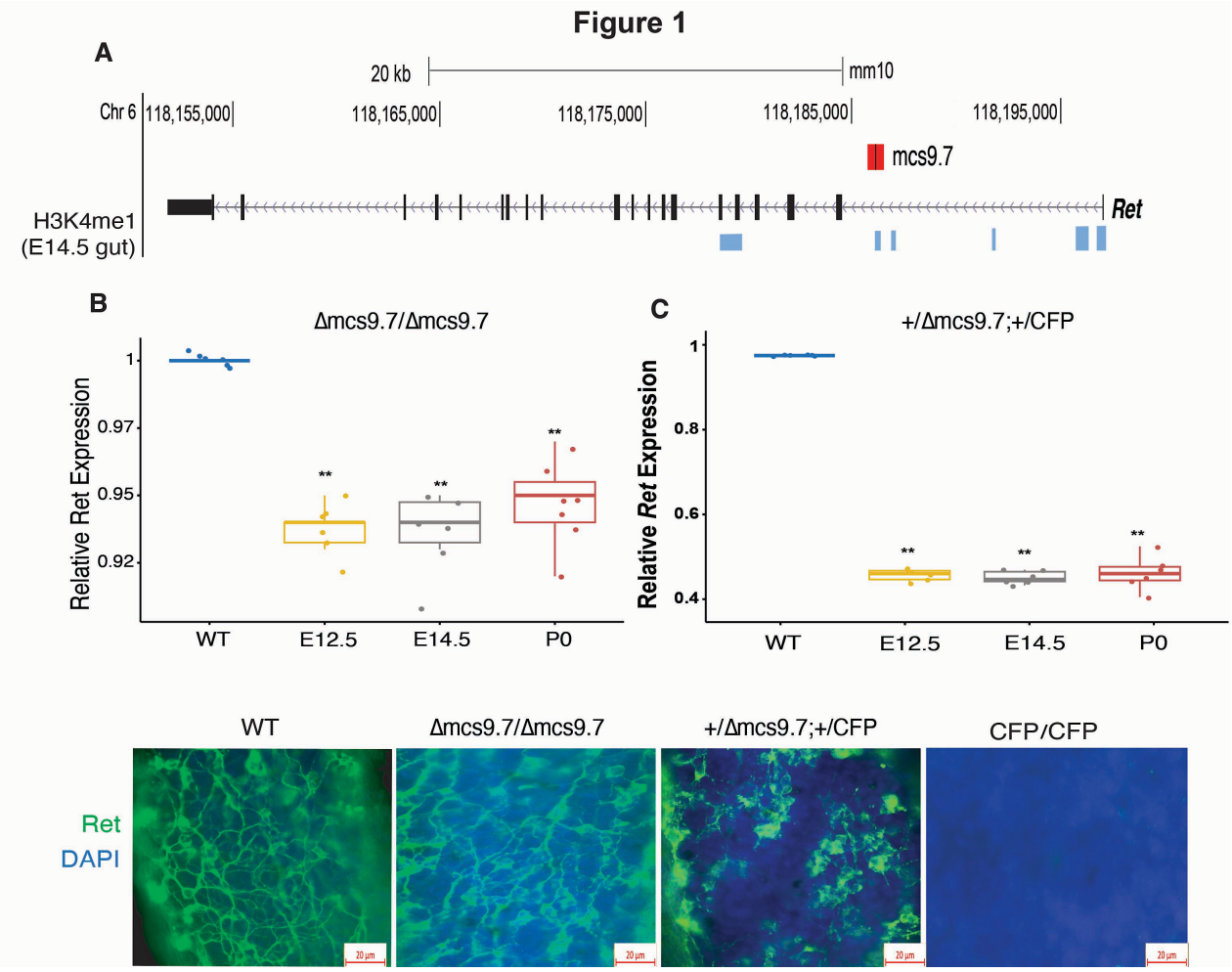

Figure 1: (A) 40kb mouse *Ret* locus (chr6:118,155,000-118,195,000; mm10) highlighting a 166bp deletion (Δmcs+9.7) of the conserved intronic *Ret* enhancer mcs+9.7. The chromatin containing mcs+9.7 is both accessible and active as revealed by H3K27ac peaks in the E14.5 mouse GI tract (data from ENCODE). **(B)** Δmcs+9.7/Δmcs+9.7; +/+ homozygotes have a ~5% reduction in *Ret* gene expression in the mouse hindgut and foregut at E12.5 and E14.5. **(C)** Double heterozygote +/Δmcs+9.7; +/CFP embryos have 45% *Ret* gene expression as compared to wildtype embryos at the same developmental times (** p<0.01). **(D)** Immunofluorescence assays for Ret in +/+; +/+, Δmcs+9.7/Δmcs+9.7; +/+, +/Δmcs+9.7/; +/CFP and +/+; CFP/CFP embryonic guts show reduction in *Ret* positive neurons in the hindgut of +/Δmcs+9.7/; +/CFP embryos at E14.5 followed by complete loss in +/+; CFP/CFP (*Ret* null) embryos. The data are presented as means with standard errors (** p<0.01; Wilcoxon rank sum test)

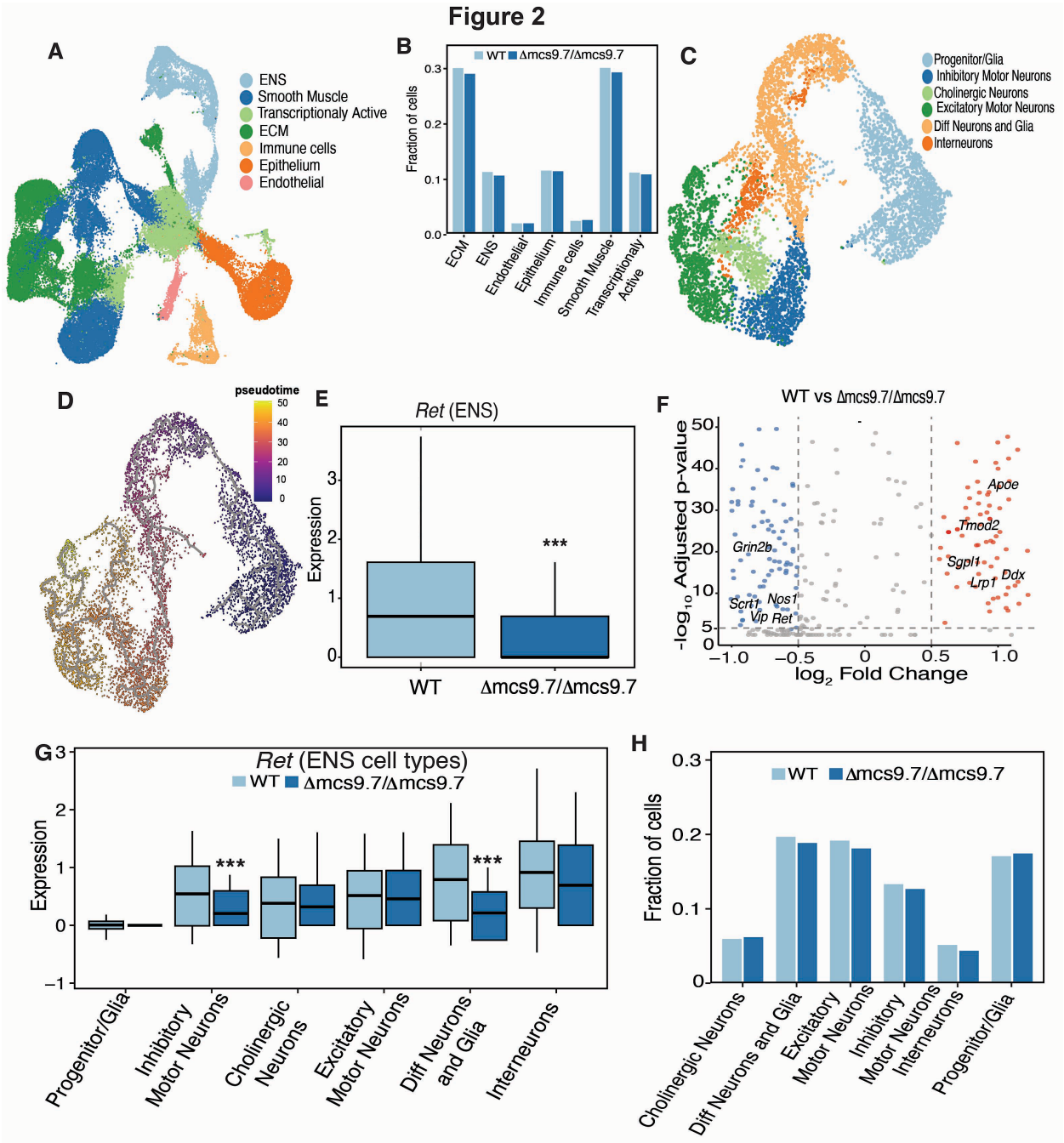

Figure 2: (A) UMAP embedding of the mouse GI tract at E14.5 colored by the 7 major cell types detected. **(B)** Homozygous loss of mcs+9.7 has no significant effect on any cell type at E14.5 (p=0.18; hypergeometric test). **(C)** ENS cells cluster into 6 major cell types/states with **(D)** a clear differentiation pathway along a defined developmental trajectory (using *Monocle*). **(E)** *Ret* gene expression is significantly diminished only in the ENS. (**F**) Differential gene expression shows significant loss of expression of key neuronal genes in

the Δmcs+9.7/Δmcs+9.7; +/+ embryos compared to wildtype. **(G)** Loss of mcs9.7 activity significantly affects *Ret* gene expression in differentiating neurons, glia and inhibitory motor neurons (** p<0.01), however, **(H)** there is no loss in cell numbers in any ENS cell type/state in Δmcs+9.7/Δmcs+9.7; +/+ embryos as compared to the wildtype. The data are presented as means with standard errors (** p<0.01; Wilcoxon rank sum test for gene expression and hypergeometric test for cell counts).

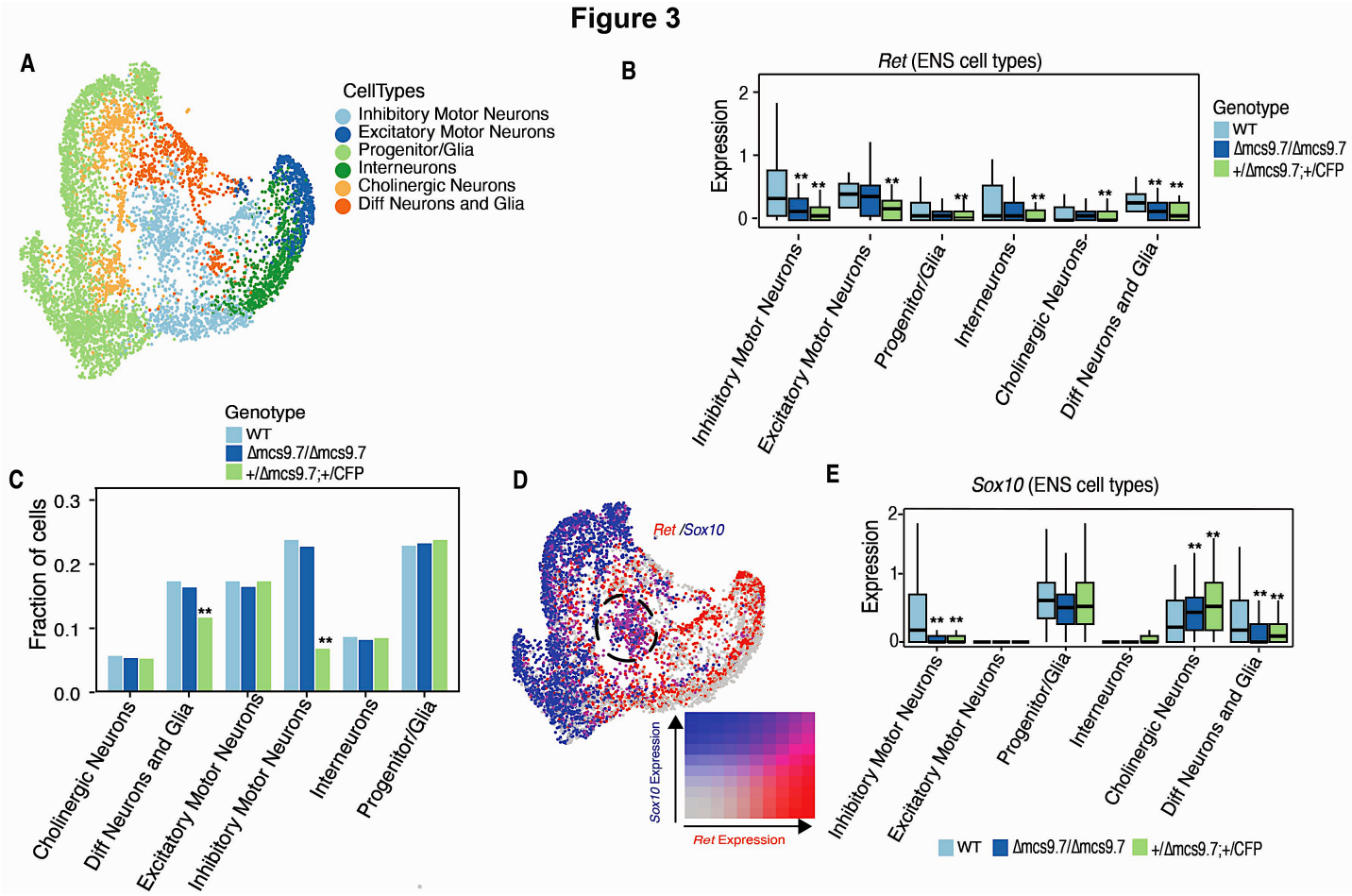

Figure 3: (A) UMAP embedding of wildtype, Δmcs+9.7 /Δmcs+9.7; +/+ and +/Δmcs+9.7/; +/CFP ENS cells at E14.5 colored by the 6 major cell types detected. (**B**) Additive loss of *Ret* expression from the coding and enhancer mutations is observed only in inhibitory motor neurons and differentiating neurons and glia. All other cell types in the +/Δmcs+9.7/; +/CFP embryos show the expected 50% reduction in expression compared to wildtype. **(C)** Inhibitory motor neurons are significantly fewer in both mutant genotypes from loss of *Ret* function in these cells. **(C)** There is significant cellular loss in both inhibitory motor neurons and differentiating neurons and glia in the +/Δmcs+9.7/; +/CFP GI tract as

compared to the wildtype. **(D)** Among all ENS cells, inhibitory motor neurons (circled), have the largest number (83%) of cells co-expressing *Ret* and *Sox10* (the transcription factor bound to mcs9.7) making it the primary cell type of action for the enhancer. (**E**) *Sox10* expression is attenuated in both inhibitory motor neurons and differentiating neurons and glia but has increased expression in cholinergic neurons (** p<0.01; Wilcoxon rank sum test for gene expression and hypergeometric test for cell counts).

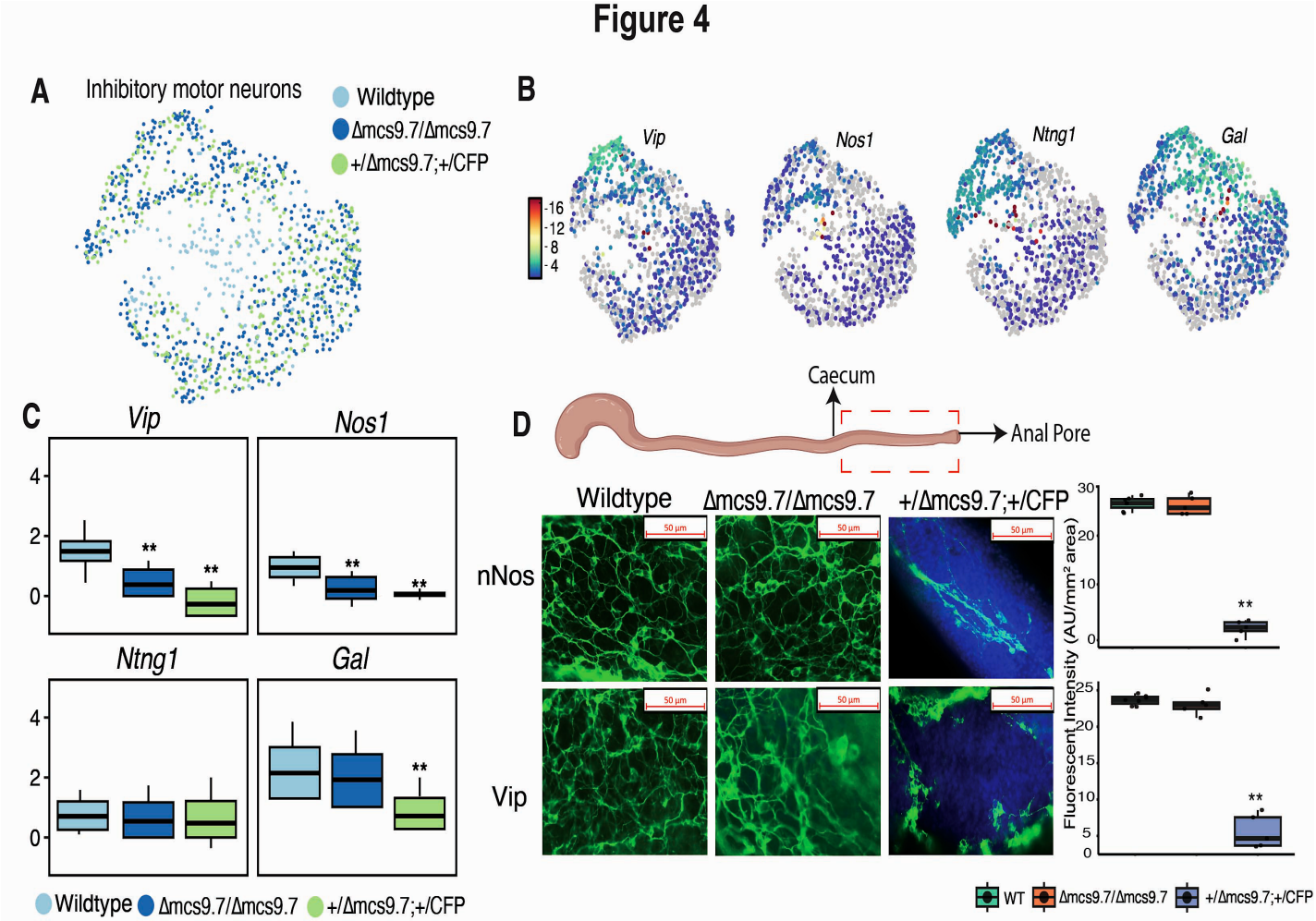

Figure 4: (A) UMAP embedding of wildtype, Δmcs+9.7 /Δmcs+9.7; +/+ and +/Δmcs+9.7/; +/CFP inhibitory motor neuron (iMNs) cells at E14.5 colored by genotype. **(B)** These cells have high expression of the classical iMN markers *Nos1, Vip, Gal* and *Ntng1* **(C)** of which *Vip, Nos1* and *Gal* are significantly (FDR<0.01) downregulated in the +/Δmcs+9.7/; +/CFP embryonic gut. **(D)** Immunofluorescence assays for nNOS and Vip in wildtype and +/Δmcs+9.7/; +/CFP embryos demonstrate a 10-fold reduction in nNOS-positive neurons and a 5-fold reduction in VIP-expressing neurons in the hindgut leading to cellular

clustering of Vip-positive neurons, a hallmark of proliferative and migratory defects (** p<0.01; Wilcoxon rank sum test for gene expression and Student's *t*-test for immunofluorescence assay).

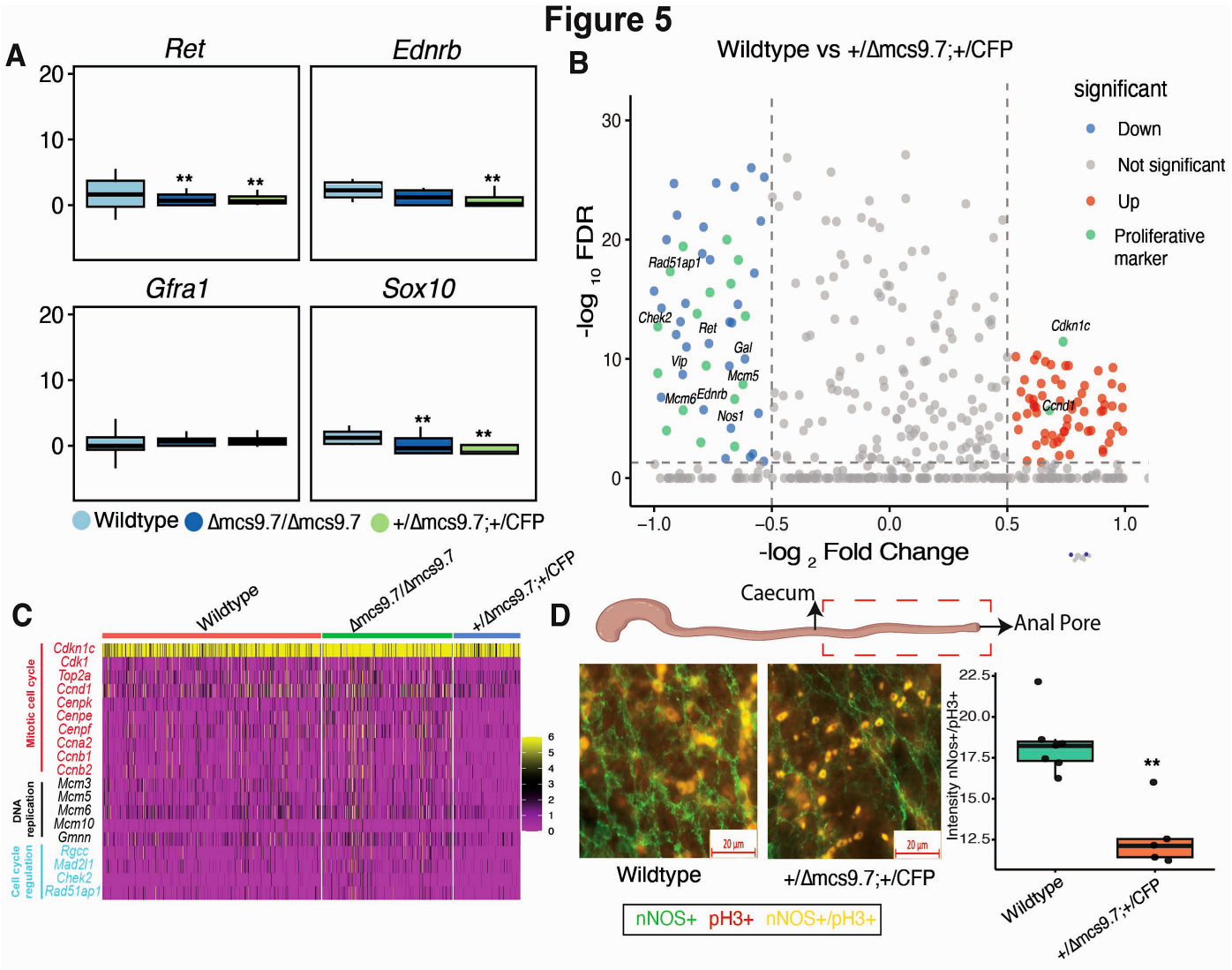

Figure 5: (A) Expression of multiple genes of the *Ret-Ednrb* gene regulatory network is affected in iMNs of both Δmcs+9.7 /Δmcs+9.7 and +/Δmcs+9.7/; +/CFP embryos. **(B)** Multiple neuronal and cell cycle regulation genes are differentially expressed in the inhibitory motor neurons of +/Δmcs+9.7/; +/CFP compared to wildtype cells. **(C)** 19 genes playing crucial roles in cell cycle regulation and DNA replication are differentially expressed in the +/Δmcs+9.7/; +/CFP embryonic gut, suggesting that the observed cellular loss is likely mediated by proliferative defects. **(D)** Immunofluorescence staining of the iMN marker nNOS and mitotic marker phosphohistone H3 (pH3) demonstrates a 54% reduction of

nNOS+/pH3+ cells highlighting loss of proliferation as the underlying mechanism of cell death (** $p<0.01$; Wilcoxon rank sum test for gene expression and Student's *t*-test for immunofluorescence assay).